Chemical Science

ROYAL SOCIETY OF CHEMISTRY

EDGE ARTICLE

View Article Online
View Journal | View Issue

Cite this: *Chem. Sci.*, 2025, **16**, 1986

All publication charges for this article have been paid for by the Royal Society of Chemistry

Received 31st July 2024
Accepted 16th December 2024

DOI: 10.1039/d4sc05097e

rsc.li/chemical-science

Probing the synergistic effects of amino compounds in mitigating oxidation in 2D $Ti_3C_2T_x$ MXene nanosheets in aqueous environments†

Jai Kumar, [ab] Jiayi Tan,[a] Razium Ali Soomro, [a] Ning Sun*[a] and Bin Xu *[a]

The shelf life of 2D MXenes in functional devices and colloidal dispersions is compromised due to oxidation in the aqueous system. Herein, a systematic investigation was carried out to explore the potential of various amino compounds as antioxidants for $Ti_3C_2T_x$ MXenes. A range of basic, acidic, and neutral amino acids were examined for their effectiveness, where certain antioxidants failed to protect MXenes from oxidation, while others accelerated their decomposition. Serine, threonine, and asparagine demonstrated excellent antioxidant activity, likely due to their evenly distributed molecular charges. These neutral amino acids outperformed glutamic acid, which possesses an electron-withdrawing COOH group, and lysine, with an electron-donating NH_2 group. Serine-functionalized MXene realized a stabilization time constant reaching 128 days, as determined by first-order reaction kinetics. Additionally, when employed as supercapacitor electrodes, aged MXene and serine-functionalized MXene exhibited specific capacitance values of 219.2 and 280.3 F g^{-1} at 5 A g^{-1} after 6 weeks, respectively. This work addresses the gap in the practical work on ionic stabilization of 2D MXenes and has significant implications for the long-term colloidal storage of MXenes using greener chemicals.

Introduction

MXenes, a group of 2D materials consisting of transition metal carbides and/or nitrides, are gaining popularity due to their attractive properties, such as hydrophobicity, diverse surface chemistry, and high electrical and thermal conductivity.[1,2] MXenes are increasingly gaining prominence in various disciplines, including biotherapy, sensors, catalysis, electromagnetic interference shielding, and energy storage.[3,4] MXenes with a generic formula of $M_{n+1}X_nT_x$[5,6] consist of n layers of carbon and/or nitrogen atoms (represented by the "X" element) with $n+1$ layers of transition metal atoms (represented by the "M" element) and T_x functional groups (–OH, –O, –F, and –Cl). Carbide MXenes, commonly produced by selective removal of the A phase from its ceramic MAX phase precursor ($M_{n+1}AX_n$, where A is an element of group 13 or 14) using hydrofluoric acid (HF) or fluoride-containing water solutions,[7] are susceptible to oxidation in the aqueous colloidal form.[8,9] This oxidation of etched MXenes in the colloidal form is a critical issue in advancing the application of MXenes to technologies that require them to be in the colloidal aqueous form.

Research indicates that MXenes undergo a chemical reaction upon contact with water and potent oxidizing agents, leading to a gradual deterioration in their structure and chemical composition, transforming Ti–C bonds into Ti–O bonds.[10,11] Investigating the oxidation process and managing the degradation of MXenes has emerged as a new research field. There is ongoing testing of rapidly advancing technologies to regulate or mitigate the aqueous colloidal oxidation of MXenes.[11–13] In terms of stability, low oxidation stability poses a significant risk to the longevity of both MXene dispersions and MXene-based devices, limiting their shelf life and overall product lifespan. To date, several investigations have verified that this oxidation leads to the deterioration of the MXene's two-dimensional structure and the decline of its functional characteristics. $Ti_3C_2T_x$ and Ti_2CT_x nanosheets, both in their colloidal form and as functional films, can undergo oxidation in an aqueous environment, forming TiO_2 and amorphous carbon.[14] The oxidation rate has been associated with temperature, pH of the solution, exposure to ultraviolet light, and the presence of chemical oxidants that produce radicals, such as ozone and hydrogen peroxide.[11,15] Apart from the dispersed nanosheets, slow degradation and worsening of electrical properties with MXene nanosheet powders and MXene-based devices have also been reported.[16] Although larger nanosheets may be more resistant to oxidation than smaller ones, according to Naguib *et al.* and others, MXene oxidation has been shown to initiate

[a]*State Key Laboratory of Organic-Inorganic Composites, Beijing Key Laboratory of Electrochemical Process and Technology for Materials, Beijing University of Chemical Technology, Beijing 100029, China. E-mail: ningsun@mail.buct.edu.cn; xubin@buct.edu.cn*

[b]*School of Energy Science and Technology, Henan University, Zhengzhou, 450046, China*

† Electronic supplementary information (ESI) available. See DOI: https://doi.org/10.1039/d4sc05097e

from the exposed edges of the nanosheet.[17–20] At the same time, the oxidation rate can significantly vary based on the intrinsic features of the nanosheet, such as surface terminal groups and defective vacancies created by Ti atoms during production.[21] In addition, MXenes with a smaller n (few atomic layers) oxidize faster than those with a larger n. For instance, based on the n layer, the oxidation trend is as follows: Ti_2CT_x > $Ti_3C_2T_x$ > $Ti_4C_3T_x$.[22,23]

A series of strategies have been devised to hinder or alleviate oxidation while storing in the colloidal state and extend the longevity of MXene-based devices. Preliminary research suggested that storage of MXene dispersions at very low temperatures (−80 °C) and in settings without oxidants, such as in vials filled with argon gas[24] can be a viable route to curb oxidation. However, these methods place restrictions on both the manufacturing of MXene and the operating conditions of MXene-based devices. Thermal annealing under inert or reductive environments can reduce the number of reactive oxygen-containing groups in MXene films, hence improving their oxidation stability.[25,26] At the same time, surface changes, such as the use of reductive di-amines as grafting intercalates, can also reduce MXene oxidation.[27] Yang *et al.* demonstrated improved stability of MXene nanosheets by *p*-iodoaniline surface functionalization and nanocomposite with conjugated microporous polymers.[28] In contrast, $Ti_3C_2T_x$ dispersed in pure water starts to undergo oxidation after a few days. Zhao *et al.* employed molecular simulations to examine the chemical relationship between $Ti_3C_2T_x$ nanosheets and antioxidants, specifically sodium L-ascorbate.[29] The simulation confirmed the steric shielding generated by the interaction of antioxidants with the nanosheets, limiting MXene-water interactions. The mechanism through which the antioxidant provides protection is currently not fully understood, and a deeper comprehension is crucial for realizing the longevity of MXene-based products.

Herein, we explore amino-acid compounds with varying chain characteristics (acidic, basic, and neutral) as competitive antioxidants to enhance the oxidation stability of $Ti_3C_2T_x$ in water. The oxidation stability of the dispersed MXene nanosheets was assessed over 6 weeks using various physical and electrochemical measurements where neutral amino molecules such as serine, threonine, and asparagine were found to be relatively potent compared to other counterparts. Interestingly, glutamic acid (acid chain) and lysine (basic chain) molecules, which have been reported as potential antioxidants, unexpectedly speed up MXene oxidation and disintegration (as illustrated in Fig. 1). The correlation between the chemical composition of an antioxidant and its performance suggests that the antioxidant's effectiveness is electrostatically driven where the ion repulsion effect is primarily responsible for imparting stability in the dispersed MXene. This study is the first to examine the impact of different amino groups and their chain structure on the oxidation stability of MXene and provides insights into the utilization of green antioxidants for the stabilization of MXene nanosheets in aqueous dispersion.

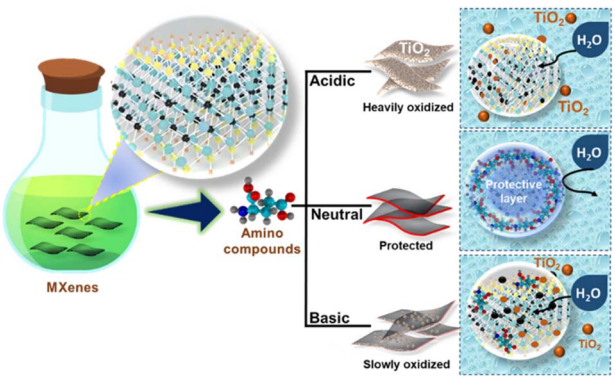

Fig. 1 Graphical representation of MXene dispersion stabilized using different kinds of amino acids.

Results and discussion

MXenes ($Ti_3C_2T_x$) were synthesized by subjecting Ti_3AlC_2 powder (Fig. S1†) to an etching process in a mixture of HCl and LiF (the details are provided in the ESI†), followed by its mixing with different amino compounds to explore the variable stability of MXene in water. During the preliminary screening, MXenes were mixed with various amino acids, including molecules with acidic, neutral, and basic properties. The main differentiation between acidic, neutral, and basic amino acids lies in their side chains and the relative proportions of amino (–NH_2) and carboxyl (–COOH) groups (as shown in Fig. S2†). For example, neutral amino compounds include equal amounts of amino and carboxyl groups. At a pH of roughly 7, the amino group accepts a proton (H^+), resulting in a positive charge (NH^{3+}), while the carboxyl group loses a proton (H^+), resulting in a negative charge (COO–). The presence of opposing charges leads to mutual annulment, resulting in an overall neutral charge for the amino acid. Acidic amino compounds are characterized by one or more extra carboxyl groups in their side chains, distinguishing them from neutral amino acids. The additional carboxyl groups enable them to readily donate protons (H^+), resulting in their acidic nature. Basic amino compounds are characterized by one or more additional amino groups in their side chains, as opposed to neutral amino acids. These extra amino groups can take protons (H^+), which gives them basic nature. To evaluate the effect of different amino acid properties on MXene oxidation stability, competitive tests were conducted using amino acids with varying characteristics. A series of neutral amino acids (serine, threonine, and asparagine), an acidic amino acid (glutamic acid), and a basic amino acid (lysine) were explored to determine which type of amino acid has the most significant impact on the oxidation stability of MXenes.

Digital imaging was used to capture the color variations of dispersions containing 0.05 mg mL^{-1} $Ti_3C_2T_x$ and various amino compounds. Fig. 2a displays the digital photographs of samples preserved for 6 weeks. As is seen, the color of freshly prepared $Ti_3C_2T_x$ MXene dispersions progressively diminishes over time, and after a week a light green color emerges compared to its fresh phase (0 week), confirming the onset of oxidation in an exposed environment. After 2 weeks, the greenish color transforms into a grey color, accompanied by the

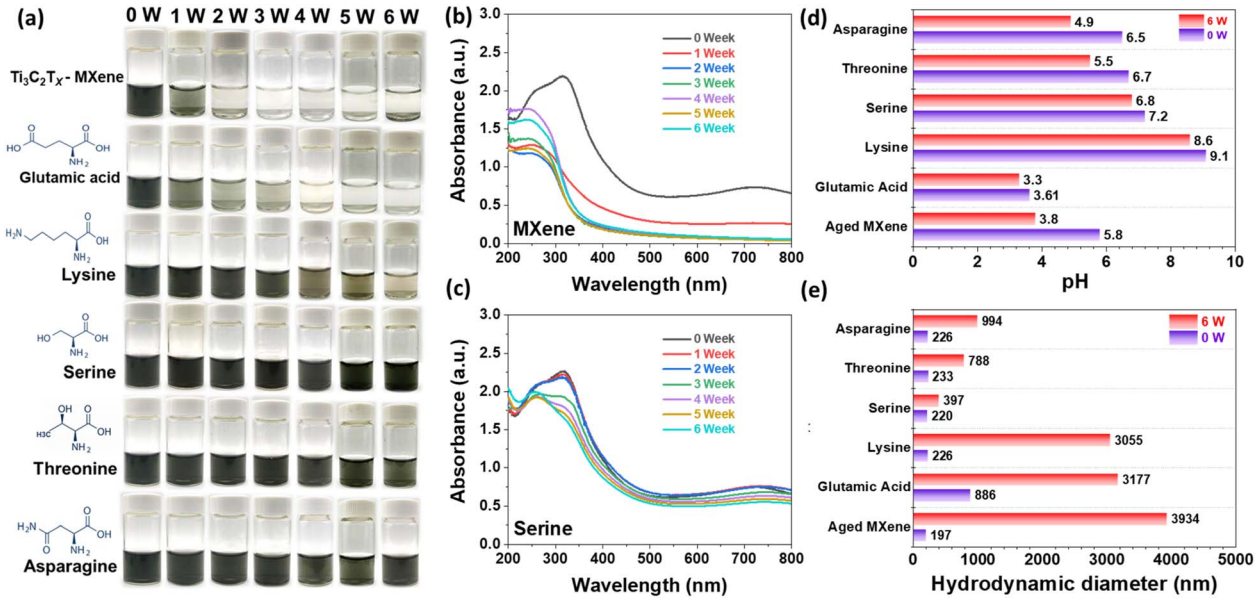

Fig. 2 (a) The visual appearance of pristine MXene and amino acid-functionalized MXene dispersion after different time intervals. UV-vis analysis of (b) fresh MXene and (c) amino acid-functionalized MXene dispersion. The change in (d) pH and (e) hydrodynamic diameter after 0 and 6 weeks of fresh MXene and amino acid-functionalized MXene dispersion.

appearance and clustering of suspended particles, confirming the loss of hydrophilicity in $Ti_3C_2T_x$ and the oxidation of Ti–C bonds into TiO_2.

This hydrolysis reaction occurs due to the combined influence of the unstable surface functionalities and interaction of exposed Ti-atoms with water molecules, deteriorating the surface from the edges towards the basal plane. This process further creates new sites that are prone to further oxidation. This hydrolysis reaction can be expressed as:

$$Ti_3C_2T_x + H_2O \rightarrow Ti_3C_2T_x\text{–}OH + H^+ \quad (1)$$

The tendency for hydrolysis has been reported to slow down in the presence of amino acids. However, the nature of the chain and its length may be critical to further controlling and molecular tuning of MXene aqueous stability. Amino compounds provide Ti–N bonds to avoid the oxidation of MXene in certain studies.[30] In this case, glutamic acid, with its acidic side chain, accelerates the oxidation compared to that of fresh MXene, where the MXene nanosheet remains stable for about one week before turning into grey sedimented particles. This change is caused by glutamic acid, which has a negatively charged side chain that leads to electrostatic repulsion between the surfaces of MXene. Even the basic amino molecule lysine fails to have a strong effect on stabilizing MXene. After 3 weeks, the MXene dispersion transitioned to a pale-yellow color, likely due to the introduction of basic functional groups during moderate oxidation, as shown in previous studies involving sodium ascorbate.[14] The NH_2 groups can act as nucleophiles, donating electron pairs to the exposed titanium atoms on the MXene surface.[31] This interaction can lead to the formation of new chemical bonds, potentially altering the surface properties of MXene and affecting its stability. Furthermore, the MXene dispersion containing lysine exhibits significant aggregation due to electrostatic repulsion, leading to the formation of aggregates of MXene flakes. Conversely, the MXene dispersion containing a neutral chain (serine, threonine, and asparagine) has a notable impact on inhibiting the hydrolysis of MXene. The color of the MXene dispersion remains consistent without any indication of agglomeration. Since neutral amino acids have no net charge, this prevents the occurrence of electrostatic repulsion between the negatively charged MXene surface and water molecules, enhancing the dispersion and contact with MXenes. All three compounds possess hydroxyl groups (OH) in their side chains, enabling them to form hydrogen bonds with functional groups on the MXene surface. To confirm this, neutral amino acids devoid of hydroxyl groups, specifically valine, were utilized as a control compared to threonine. Valine, lacking hydroxyl groups, cannot form hydrogen bonds with MXene, reducing contact and stability. The color of MXene gradually decreased over time due to its oxidation (Fig. S3a†), as evidenced by the development of TiO_2 particles observed in the SEM image and the corresponding peaks in XRD patterns (Fig. S3(b and c)†).[32] These findings support the hypothesis that hydroxyl groups in amino acids are crucial for the stability of MXene. This direct coupling can enhance the stability of the MXene. Preliminary findings confirm that the neutral chain can strongly adhere to the oxidation-prone locations on $Ti_3C_2T_x$ nanosheets. This allows for effectively preserving MXene nanosheets and prolonging their colloidal stability. This confirms that the stability of MXene is significantly influenced by the nature of amino acids (acidic, basic, or neutral), as depicted in Fig. 1.

Fig. 2(b and c) compares the UV-vis spectra of $Ti_3C_2T_x$ dispersion containing various amino compounds. The UV-vis spectra of fresh MXene exhibit three distinct peaks at

wavelengths of 250, 310, and 745 nm, respectively. As aging progresses, the intensity of the 310 and 745 nm peaks declines, while the intensity of the first characteristic peak increases. Additionally, the TiO_2 characteristic peak aligns with the first characteristic peak at a wavelength of 249 nm. The second peak vanished after 1 week, whereas the third peak vanished after 2 weeks. On the other hand, the absorbance of the glutamic acid dispersion diminishes similarly to that of fresh MXene (Fig. S4†). There is a rapid decrease in the absorbance peak at 745 nm and 310 nm, with the emergence of a strong peak in the lower absorbance area (250 nm) after 2 weeks. Similarly, MXene dispersion remains intact for up to 3 weeks when lysine is present. However, after 4 weeks, the absorbance peaks of the MXene start to distort due to oxidation. UV-vis analysis reveals that the neutral chain-based amino compound exhibits encouraging antioxidant characteristics. Out of serine, threonine, and asparagine, serine exhibits a significant antioxidant impact where the absorbance intensity in both the lower and higher regions is effectively preserved. Threonine and asparagine exhibited a comparable effect to serine; nevertheless, their absorbance intensity slightly decreases at 310 nm. However, peak deformation is not detected, suggesting that neutral amino compounds are more efficient than their reactive counterparts.

The first-order kinetic technique was employed to assess the rate of oxidation. The change in concentration over time was determined by measuring the intensity at a characteristic peak of 746 nm. The change in absorbance as a function of time at 746 nm and the oxidation kinetics equation were fitted to the data. Fig. S5a† shows a significant drop in the normalized intensity ratio of fresh MXenes, glutamic acid, and lysine. Additionally, their oxidation degradation percentages reached 93%, 90%, and 83%, respectively. However, serine, threonine, and asparagine exhibit a modest decrease in their normalized value, with their oxidative degradation percentages reaching 25%, 29%, and 32%, respectively. This further validates the exceptional antioxidant capabilities of serine dispersion. In addition, the time decay constant was determined using the following equation:[33]

$$A = A_{\text{unoxd}} + A_{\text{re}}e^{(-t/\tau)} = A_{\text{unoxd}} + A_{\text{re}}e^{(-kt)} \quad (2)$$

where A, A_{unoxd}, and A_{re} denote the absorbances of $Ti_3C_2T_x$ dispersions after a pre-set aging interval, unreacted and reacted analogs, respectively; t denotes the oxidation time (day); τ signifies the decay constant denoting the time required for MXene decay, while k represents the reaction rate constant.

Fig. S5b† shows that MXene exhibits a high oxidation rate for nearly 7 days. In the case of amino acids, the τ values for glutamic acid and lysine are 12 and 35 days, respectively, which align well with UV-vis analysis results, whereas serine, threonine, and asparagine exhibit τ values of 128, 110, and 96 days, respectively. They confirm that neutral amines (serine, threonine, and asparagine) were ineffective towards oxidation stability, and the resulting MXene dispersion subsequently realized the formation of TiO_2 within approximately one week. This is attributed to weak non-covalent interactions with MXenes rather than bond formation. The neutral amino acid-functionalized MXene performs well, in agreement with the reported work (Table S1†).

Fig. 2d demonstrates that the pH of the fresh MXene dispersion decreases, while serine maintains a neutral pH in the system using consistent ionization equilibrium, providing further evidence that MXene can be efficiently and stably stored in the presence of serine compared to other amino acids. The oxidation of MXene dispersions leads to a reduction in the pH of the solution, likely due to the detachment of surface functional groups, such as fluorine, which react with water to form corresponding acids, thereby releasing H^+ ions. Additionally, the interaction between carbon and oxygen atoms on the MXene surface can generate carbon dioxide (CO_2), which subsequently dissolves in water, forming carbonic acid (H_2CO_3).[34] These processes contribute to the overall acidification of the dispersion. Previous studies indicate that hydrolysis may reduce the pH, particularly in titanium-based MXenes. This process results in the generation of titanium dioxide on the surface, deteriorating the MXene compositional characteristics.[35,36] Dynamic light scattering (DLS) analysis confirmed the change in particle size distribution of MXene dispersion. Fig. 2e shows that the initial hydrodynamic particle size of the fresh MXene was 197 nm, which, after 6 weeks, reached a maximum of 3934 nm. However, the hydrodynamic volume of functionalized MXenes also increased, attributed to amino moieties. The change in volume expansion was relatively smaller compared to the fresh MXenes. After 6 weeks, the mean hydrodynamic size of glutamic acid and lysine dispersions reached 3177 and 3055 nm, respectively, comparable to that of aged MXene. On the other hand, the average hydrodynamic size of serine dispersions remains relatively unchanged, suggesting a consistent and steady behavior. This confirms that the oxidation of MXene is accompanied by the consumption of surface hydroxyl groups (–OH). In contrast, these functional groups enhance hydrophilicity when MXene is functionalized with new groups, such as carboxylic acid (COOH) or carbonyl (C=O) groups.[37] This increased hydrophilicity promotes the formation of a hydration layer around the MXene particles. Consequently, the formation of this hydration layer results in an increase in the hydrodynamic diameter.[38] As a result, the hydrodynamic diameter of oxidized MXene is significantly larger than that of the control sample.

Oxidation can potentially induce defects and disorder in the structure of MXene, resulting in a decrease in overall crystallinity.[39] This event can potentially amplify the existing crystal peaks while diminishing their strength. Alternatively, it may also induce the emergence of new peaks associated with secondary phases, such as anatase or rutile nanoparticles of titanium oxide.[26] Fig. 3a shows the presence of (002) plane peaks in MXene, suggesting that the MXene has been successfully derived from the MAX phase. The functionalized MXene exhibits a similar profile, however, with a slight shift in the (002) peaks, reflecting the interaction of antioxidants with the MXene surface, resulting in an enlarged interlayer gap. Enhancing the interlayer gap could facilitate the incorporation of higher ions into the MXene structure, potentially enhancing MXene's

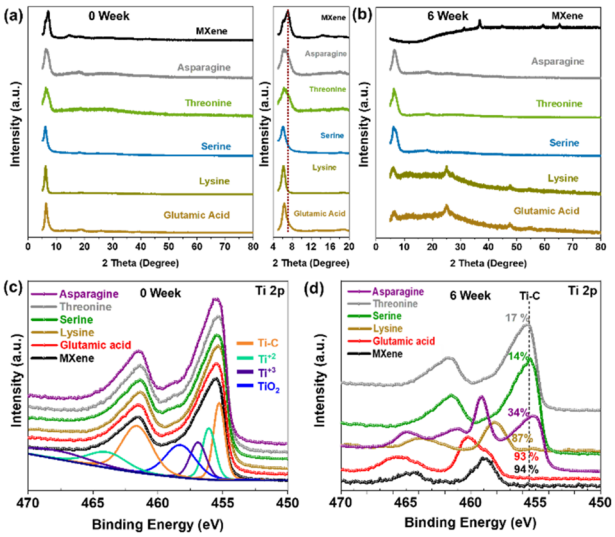

Fig. 3 The XRD analysis of fresh MXene and amino acid-functionalized MXene after (a) 0 and (b) 6 weeks. The deconvoluted XPS spectra of Ti 2p unprotected and protected MXene films after (c) 0 and (d) 6 weeks of aging.

energy storage performance. Following a storage period of 6 weeks, the MXene (002) peak vanishes, and other peaks emerge, potentially indicating the presence of titanium oxide (either anatase or rutile), as depicted in Fig. 3b. Similarly, the MXene films containing glutamic acid and lysine exhibit no typical (002) peak, confirming complete oxidative degradation of MXene. Whereas films produced *via* neutral chain amino molecules exhibit unaltered behavior, indicating a strong effect in stabilizing the crystallographic structure of MXene.

X-ray photoelectron spectroscopy (XPS) further confirmed the change in chemical composition of the MXene surface. Fig. S6† displays the XPS survey spectra of the $Ti_3C_2T_x$ and amino-functionalized MXene samples. Compared to fresh MXene samples, which exhibit typical Ti 2p, C 1s, and O 1s profiles, the functionalized MXenes showed a new peak corresponding to nitrogen (N 1s) in the 396–401.25 eV region. The peak's position and shape provide insights into the nature of the bonding between the amine group and the MXene surface. Fig. 3(c) and S7† display high-resolution Ti 2p XPS spectra of MXene-amino acids and pure MXene for 0 week, exhibiting two distinct peaks separated by approximately 5.9 eV due to spin–orbit coupling. The observed peaks are attributed to the core electrons, specifically the Ti $2p_{3/2}$ (with a greater binding energy) and Ti $2p_{1/2}$ orbitals. The precise binding energy of the Ti $2p_{3/2}$ peak functions is a distinctive characteristic for determining the oxidation state of titanium. The Ti $2p_{3/2}$ peak detected at approximately 455.54 eV indicates titanium in a reduced oxidation state, such as Ti^{3+}, aligning with the mixed oxidation states commonly found in MXenes. After the pristine MXene is subjected to amine functionalization, the introduced amine groups ($-NH_2$) lowers the binding energies of the Ti 2p peaks. The Ti $2p_{3/2}$ peaks for glutamic acid, lysine, serine, threonine, and asparagine are noted at 455.40, 455.37, 455.35, 455.39, and 455.43 eV, respectively. The slight shift in each case is ascribed to the electron-donating characteristic of the amine groups, facilitating the removal of the Ti 2p core electrons and leading to a decrease in binding energy and, thus, the formation of Ti–N coordination bonds.

After 6 weeks, the MXene, glutamic acid and lysine samples exhibit significant oxidation and the emergence of TiO_2 peaks (Fig. 3d and S8†). The peaks exhibit a distinct and precise shape, suggesting that the oxidation status of titanium inside the MXene is very uniform. The presence of glutamic acid and lysine amino acids indicates that their carboxylic acid (–COOH) and amine ($-NH_2$) groups enable them to engage with exposed titanium atoms on the MXene surface by interaction, establishing interactions with a central metal ion. Consequently, the titanium atoms would become more vulnerable to being attacked by other oxidizing substances, such as water (H_2O) or dissolved oxygen (O_2) in the surrounding environment. Conversely, neutral chain dispersions exhibit a notable ability to resist oxidation, even after 6 weeks. This effect is particularly evident for serine and threonine, whereas no distinct peaks of TiO_2 were detected in serine and threonine after 6 weeks. However, a minor elevation in TiO_2 peaks was seen in asparagine, suggesting its partial oxidation, and the Ti–C peak degraded up to 34%. The presence of hydroxyl (–OH) functional groups in amino acids such as serine and threonine, or an amide ($-CO-NH_2$) group in asparagine, may result in weaker interactions with the MXene surface compared to glutamic acid and lysine. This weaker interaction is unlikely to significantly weaken the Ti–O bonds, thus hindering the oxidation process. The FWHM for Ti $2p_{1/2}$ is found to be within the range of 1.5–2.5 eV, which is typical for TiO_2 and is consistent with the literature (Fig. S7 and S8†).[40,41] However, we acknowledge that some peaks may appear broader due to overlapping contributions from surface states or minor Ti sub-oxides, which are challenging to resolve clearly in highly oxidized environments.

The C 1s spectra of the original MXene and the amino acid-functionalized MXene are shown in Fig. S9.† Typically, the C 1s spectrum of fresh MXene displays peaks resulting from various carbon bonding conditions (Fig. S9a†). In its original/fresh state, MXene has a distinct peak at 282.19 eV, indicating carbon atoms directly linked to titanium atoms in the MXene lattice. These carbon atoms form carbide groups known as Ti–C. In the amino acid-functionalized MXene, an extra C–N bond around ~286 eV (Fig. S9(b–f)†), ranging from 15 to 13.92 atom%, is evident. This bond indicates the direct connection between carbon and nitrogen atoms in the amine functional groups (C–N). Consequently, a small change was seen in the Ti–C peak for glutamic acid, lysine, serine, threonine, and asparagine at 282.11, 281.95, 282.03, 281.99, and 282.01 eV, respectively. The presence of amino groups may decrease the intensity of the carbide peak (C–Ti) since they effectively replace or partially cover some surface titanium carbide groups. After 6 weeks of storage, the C 1s XPS spectrum of MXene shows significant changes due to oxidation (Fig. S10†). The content of C–C increased to 76.1 atom%, indicating the occurrence of oxidation and the production of amorphous carbon. Similarly, glutamic acid and lysine exhibit oxidation behavior similar to that of oxidized MXene. Furthermore, the intensity of the C–O

peak was enhanced due to the oxidation of some carbide groups (C–Ti) to generate novel C–O functionalities.[42] However, serine, threonine, and asparagine demonstrate the presence of C–Ti, C–Ti–O, C–C, C–N, C–O, and O–C=O bonds, suggesting that $Ti_3C_2T_x$ exhibits a favorable protective effect (Fig. S10(d–f)†).

Furthermore, the O 1s spectrum shows distinct binding energies, indicating diverse chemical surroundings of oxygen atoms on the MXene surface (as illustrated in Fig. S11a†). A peak at about 530–532 eV suggests the existence of oxygen atoms bonded with metal atoms in the MXene structure, usually titanium (Ti–O). Furthermore, the presence of a signal at 532.7 eV indicates the presence of oxygen atoms attached to hydroxyl groups (–OH) on the surface of the MXene. The hydroxyl groups may originate from either the etching process or exposure to water vapor afterward. Following functionalization, an increase in the peak C–Ti–$(OH)_x$ (Fig. S11(b–f)†) is evident, which is attributed to the reaction between primary or secondary amines ($–NH_2$) in amino compounds and the surface functional groups on MXene, specifically surface oxides or adsorbed water molecules. Fig. S12(a–c)† demonstrates noticeable TiO_2 formation after 6 weeks in aged MXene consisting of glutamic acid and lysine. The following reaction validates the conversion of the Ti–C backbone to TiO_2, as exemplified by the conversion of $Ti_3C_2O_2$.[33]

$$Ti_3C_2O_2 + 4H_2O \rightarrow 3TiO_2 + 2C + 4H_2 \quad (3)$$

On the other hand, the MXene dispersion with neutral amino acid exhibits no noticeable alteration in the O 1s spectra even after 6 weeks (Fig. S12(d–f)†). This indicates that the neutral chain molecules effectively maintain the stability of the Ti–C structure without transforming TiO_2. Among various neutral amino groups, serine exhibits greater stability without the loss of surface (–OH) groups; however, threonine and asparagine demonstrate a decline in surface group presence.

Fig. S13† shows that all samples exhibit a prominent N 1s peak, confirming the interaction of the amino group with $Ti_3C_2T_x$. The C–N peak, found between 401 and 404 eV, indicates nitrogen atoms bound to carbon atoms in the amino groups (C–N bonds). This peak is most noticeable and significant in amino-functionalized MXene films. An elevated binding energy peak (about 399–401 eV) could suggest the existence of protonated amine groups ($–NH_3^+$). This phenomenon arises when the amino groups on the MXene surface come into contact with acidic protons, either from the MXene surface itself or from the surrounding environment.[43] Furthermore, it was discovered that the MXene-amino group exhibits a weak N–Ti bond at approximately 396 eV, providing further evidence of the N–T bond. Fig. S14(a and b)† illustrates the N 1s spectra of glutamic acid and lysine after 6 weeks. The disappearance of the N 1s peak can be attributed to the gradual desorption of amino acid molecules from the MXene surface, leading to a decrease in nitrogen concentration. However, after 6 weeks, serine, threonine, and asparagine displayed a distinct N 1s peak (Fig. S14(c–e)†), suggesting the presence of a stable nitrogen-containing group.[11]

FTIR analysis further assessed the interaction of $Ti_3C_2T_x$ and added antioxidants (Fig. S15†). Pristine MXene shows distinctive peaks that represent its surface functional groups: The broad peaks at 3000–3600 cm^{-1} represent O–H stretching vibrations from hydroxyl groups (–OH) on the MXene surface, a result of the etching process; the peak in the 1600–1500 cm^{-1} range is attributed to C=O stretching vibrations from residual surface functional groups like carboxyl groups (–COOH) or carbonyl groups (C=O). In the case of amino acid-functionalized MXenes, N–H stretching vibrations were found between 3600 and 3650 cm^{-1}, while N–H bending vibrations were between 1525 and 1550 cm^{-1}. Additionally, the stretching vibrations of the amide group (–NH–CO–) were observed between 1575 and 1600 cm^{-1}. The presence of NH bonding with MXenes confirms the successful functionalization of MXenes with amino acids.

Scanning electron microscopy (SEM) was used to analyze the surface morphology of pristine MXene and amino acid-functionalized films to determine the degree of oxidation, as illustrated in Fig. 4. The film's physical characteristics following vacuum filtration are also provided. Once vacuum-dried, all samples display a smooth, sheet-like appearance. The surface of MXene and amino acid-functionalized films is smooth and flat, as seen by the SEM images. Following 6 weeks, glutamic acid and lysine films show evidence of oxidation, resulting in an altered morphology from sheet-like structures to nanoparticles with noticeable voids and fractures. These changes may be attributed to the aggregation of inflexible TiO_2 particles. On the other hand, the surface of MXene functionalized with neutral amino acids is characterized by wrinkles but without any deformation. In particular, serine exhibits a highly smooth surface, further confirmed by comparing its cross-section to other counterparts.

The extent of interlayer oxidation was examined using cross-sectional analysis, as depicted in Fig. 5 and S16.† MXene exhibits a distinct layered stacking structure (Fig. S16a†), which becomes distorted and oxidized to TiO_2 after 6 weeks of storage (Fig. 5a). This process leads to the destruction of MXene's

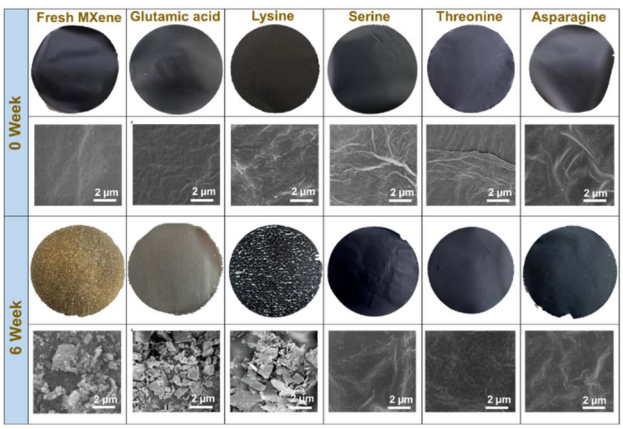

Fig. 4 Pictures of membrane sheets and the corresponding SEM images of fresh MXene and amino acid-functionalized MXene after 0 and 6 weeks of aging.

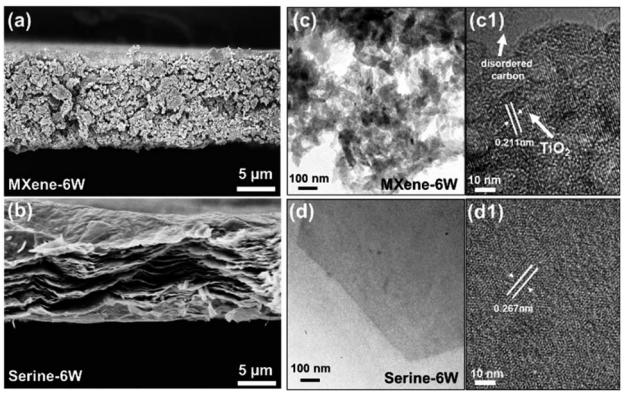

Fig. 5 The cross-sectional SEM images of (a) fresh MXene and (b) serine-functionalized MXene after 6 weeks of aging. TEM images of (c) fresh MXene and (d) serine-functionalized MXene along with their (c1 and d1) HR-TEM images after 6 weeks of aging.

unique structure and ultimately results in pulverization. This is unlike serine-functionalized MXene, which maintains its layered structure after 6 weeks without any aggregation or TiO_2 particle formation (Fig. 5b).

High-resolution transmission electron microscopy (HRTEM) further elucidates the change in the MXene crystal structure with different antioxidants. Different layers exhibit distinct separation, with the MXene and MXene-serine samples showing flat, two-dimensional sheets with a smooth surface appearance on day 1 (0 weeks) (Fig. S17†). Furthermore, freshly synthesized MXene exhibits visible well-exfoliated 2D nanosheets with an inter-space of 0.256 nm, representing the distance between neighboring ordered structures (Fig. S17a†). After a storage period of 6 weeks, the MXene film exhibited the presence of TiO_2 particles with disordered carbon (Fig. 5c), confirming a significant level of oxidation. As a result, the MXene layers become more susceptible to breaking down into smaller fragments. However, in the case of serine functionalization, the lamellar structure remains intact with a lateral dimension that is equal to that of the original MXene even after 6 weeks (Fig. 5d). The interlayer spacing of 0.267 nm resembles that observed in freshly exfoliated nanosheets (Fig. 5d1). The comparison of morphological features at the micro-/nanoscale indicates that serine is an effective antioxidant material for the extended preservation of MXene.

The evaluation of serine adsorption on the electrochemical activities of functionalized MXene depends extensively on the change in electrical conductivity. Fig. 6a presents the changes in normalized conductivity (σ/σ_o) for the $Ti_3C_2T_x$ film and its serine counterpart at various time intervals. The quick decrease in the σ/σ_o ratio of pristine $Ti_3C_2T_x$ during 6 weeks can be attributed to the semiconductor nature of the resulting TiO_2 and the increase in Joule heat caused by intensified electron collisions due to the collapsed Ti–C backbone.[44] The process of restacking can cause a reduction in the efficiency of the electron transport network, which may also lead to a loss in conductivity. In the case of serine-functionalized MXene, a minimal decline in σ/σ_o over time further validates that serine molecules can act

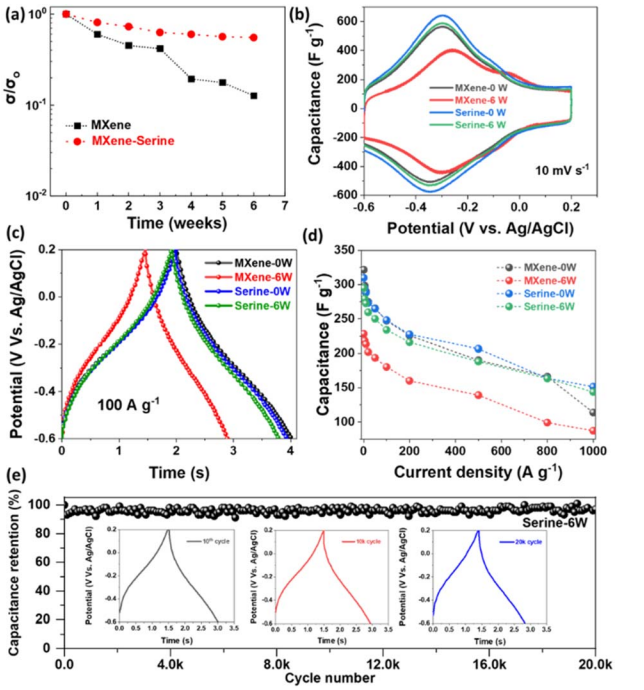

Fig. 6 (a) Normalized conductivity profiles of fresh MXene and serine-functionalized MXene after different aging times. (b) CV profiles of fresh MXene and serine-functionalized MXene after 0 and 6 weeks of aging time at a fixed scan rate of 10 mV s^{-1}. (c) Charge–discharge curves of pristine MXene and serine-functionalized MXene after 0 and 6 weeks of aging time at a fixed current density of 100 A g^{-1}. (d) Specific capacitances of pristine MXene and serine-functionalized MXene after 0 and 6 weeks of aging time at different current densities. (e) Cycling performances of the MXene-serine film after 6 weeks at 100 A g^{-1}.

as a protective barrier, slowing down the rate at which oxygen and vapor interact with the MXene surface.

The electrochemical performance of the $Ti_3C_2T_x$ dispersion was evaluated using direct vacuum-filtering of the MXene and MXene-serine dispersion into usable film electrodes for supercapacitors (0 and 6 weeks) in a three-electrode system with 3 M H_2SO_4 electrolyte. MXenes have surface functional groups, such as hydroxyl (–OH) or oxygen (–O) groups, and surface defects that can engage in redox reactions with the electrolyte ions. The CV-based pseudocapacitive energy storage behavior of serine-functionalized MXene and fresh $Ti_3C_2T_x$ films is shown in Fig. 6b and S18,† where the redox couple can be seen at −0.07 V (oxidation) and −0.2 V (reduction) in the potential of −0.6 to 0.2 V *versus* Ag/AgCl at a scan rate of 10 mV s^{-1}. Both fresh and serine-functionalized MXene exhibit a typical curve at various scan rates for 0 week (Fig. S18(a and c)†). The slightly increased capacitance in serine-based samples relative to that in pristine MXene indicates that the interaction between serine and MXene facilitates surface functionalization, thereby introducing new active sites for charge storage. Additionally, combining MXene and serine may produce synergistic effects, improving the electrochemical performance. After 6 weeks, the aged MXene exhibits an irregular redox peak and a decreased total capacitive area (Fig. 6b), suggesting decreased site availability for ion

adsorption/desorption and possibly impeded surface redox reactions owing to oxidation. However, even after 6 weeks, overlapping CV curves were observed in the case of serine, confirming that $Ti_3C_2T_x$ nanosheets are well-preserved with no alteration in their energy-storage characteristics (Fig. S18d†). Fig. 6c and S19† illustrate the galvanostatic charge–discharge behavior of the MXene and serine films after 0 and 6 weeks. Both samples exhibited a non-linear curve in their galvanostatic charge–discharge behavior with nearly identical discharge times for both protected and unprotected MXene. However, after 6 weeks, the discharge time for unprotected MXene significantly decreases. Conversely, the MXene with serine protection exhibits unaltered characteristics and provides a discharge time comparable to that of the original MXene. This suggests that serine has the potential to be an effective antioxidant without compromising MXene's electrochemical behavior. The galvanometric specific capacitance of the prepared MXene was assessed, as depicted in Fig. 6d. The initial capacitance values of the fresh MXene were measured at 298.1, 290.8, 277.2, 267.3, 252.7, 223.1, 193.3, 164.1, and 112.6 F g^{-1} for current densities of 5, 10, 30, 50, 100, 200, 500, 800, and 1000 A g^{-1}, respectively. The serine-functionalized MXene films exhibited specific capacities of 294.3, 288.2, 273.7, 265.2, 248.1, 226.3, 207.2, 166.3, and 152.6 F g^{-1} at current densities of 5, 10, 30, 50, 100, 200, 500, 800, and 1000 A g^{-1}, respectively. As is seen, unprotected MXene exhibits a decline in its galvanometric capacitance behavior after 6 weeks. The capacitance values at different current densities are as follows: 219.2, 213.2, 202.5, 193.8, 179.1, 159.5, 138.1, 99.2, and 85.1 F g^{-1} at 5, 10, 30, 50, 100, 200, 500, 800, and 1000 A g^{-1}, respectively. In contrast, protected MXene has comparable capacitance behavior, with values of 280.3, 271.6, 260.5, 250.1, 232.7, 216.4, 187.3, 163.2, and 143.1 F g^{-1} achieved at 5, 10, 30, 50, 100, 200, 500, 800, and 1000 A g^{-1}, respectively. Fig. 6e illustrates the extended cycling performance of the MXene-serine film at a current density of 100 A g^{-1}. The film has a capacitance retention of 90.31% after undergoing 20 000 cycles. The charge/discharge curves for the first and last cycles show comparable profiles with minimal distortion, indicating its exceptional cycling endurance and reversibility.

Conclusions

This work presents a straightforward and efficient method for stabilizing $Ti_3C_2T_x$ aqueous colloids using different amino acids as antioxidants. A series of experiments involving several amino acids, including basic (lysine), acidic (aspartic acid), and neutral (serine, threonine, and asparagine), were systematically investigated to assess their efficacy in inhibiting oxidation of MXene in an aqueous system. The comparative assessment indicates that neutral amino acids are highly efficient in safeguarding oxidation-susceptible areas on $Ti_3C_2T_x$ nanosheets by establishing a well-balanced contact with the surface, avoiding excessive and insufficient binding. This characteristic enables them to exhibit high resistance to oxidation and exceptional dispersibility. Serine showed remarkable antioxidation efficiency with optimal colloidal stability for 128 days. Moreover, serine-functionalized MXene retained its electrochemical performance after 6 weeks, while the untreated MXene had a considerable loss in specific capacitance and electrochemical characteristics. This work addresses the issue of effectively stabilizing 2D MXenes in aqueous systems, with practical ramifications for preserving these materials over time without oxidation or loss of chemical potential.

Data availability

The data supporting this article have been included as part of the ESI.†

Author contributions

Jai Kumar: conceptualization, methodology, and writing the original draft. Jiayi Tan: investigation and methodology. Razium Ali Soomro: investigation, formal analysis, and writing the original draft. Ning Sun: investigation, formal analysis, writing – review & editing. Bin Xu: writing – review & editing, supervision, project administration, and funding acquisition.

Conflicts of interest

There are no conflicts to declare.

Acknowledgements

This work was financially supported by the National Natural Science Foundation of China (Grant No. U2004212) and the Fundamental Research Funds for the Central Universities (buctrc202141).

References

1 R. Qin, G. Shan, M. Hu and W. Huang, *Mater. Today Phys.*, 2021, **21**, 100527.
2 M. A. Ahouei, T. H. Syed, V. Bishop, S. Halacoglu, H. Wang and W. Wei, *Catal. Today*, 2023, **409**, 162–172.
3 X. Zhu, Y. Zhang, M. Liu and Y. Liu, *Biosens. Bioelectron.*, 2021, **171**, 112730.
4 L. Bharali, J. Kalita and S. Sankar Dhar, *ChemistrySelect*, 2023, **8**, 202301486.
5 X. Li, Z. Huang and C. Zhi, *Front. Magn. Mater.*, 2019, **6**, 312.
6 Y. Wei, P. Zhang, R. A. Soomro, Q. Zhu and B. Xu, *Adv. Mater.*, 2021, **33**, 2103148.
7 A. Zhou, Y. Liu, S. Li, X. Wang, G. Ying, Q. Xia and P. Zhang, *J. Adv. Ceram.*, 2021, 1–49.
8 F. Cao, Y. Zhang, H. Wang, K. Khan, A. K. Tareen, W. Qian, H. Zhang and H. Ågren, *Adv. Mater.*, 2022, **34**, 2107554.
9 J. Wozniak, M. Petrus, T. Cygan, A. Lachowski, M. Kostecki, A. Jastrzębska, A. Wojciechowska, T. Wojciechowski and A. Olszyna, *Materials*, 2021, **14**, 6011.
10 X. Wang, Z. Wang and J. Qiu, *Angew. Chem.*, 2021, **133**, 26791–26795.

11 S. Athavale, S. Micci-Barreca, K. Arole, V. Kotasthane, J. Blivin, H. Cao, J. L. Lutkenhaus, M. Radovic and M. J. Green, *Langmuir*, 2023, **39**, 918–928.
12 I. Persson, J. Halim, T. W. Hansen, J. B. Wagner, V. Darakchieva, J. Palisaitis, J. Rosen and P. O. Persson, *Adv. Funct. Mater.*, 2020, **30**, 1909005.
13 M. W. Barsoum and Y. Gogotsi, *Ceram. Int.*, 2023, **49**, 24112–24122.
14 X. Guo, J. Zhang, J. Song, W. Wu, H. Liu and G. Wang, *Energy Storage Mater.*, 2018, **14**, 306–313.
15 C. Shi, C. Li, Y. Wang, J. Guo, S. Barry, Y. Zhang and N. Marmier, *Water*, 2022, **14**, 2309.
16 Q. Yang, S. J. Eder, A. Martini and P. G. Grützmacher, *npj Mater. Degrad.*, 2023, **7**, 6.
17 F. Xia, J. Lao, R. Yu, X. Sang, J. Luo, Y. Li and J. Wu, *Nanoscale*, 2019, **11**, 23330–23337.
18 Y. Lee, S. J. Kim, Y. J. Kim, Y. Lim, Y. Chae, B. J. Lee, Y. T. Kim, H. Han, Y. Gogotsi and C. W. Ahn, *J. Mater. Chem. A*, 2020, **8**, 573–581.
19 Y. Chae, S. J. Kim, S.-Y. Cho, J. Choi, K. Maleski, B.-J. Lee, H.-T. Jung, Y. Gogotsi, Y. Lee and C. W. Ahn, *Nanoscale*, 2019, **11**, 8387–8393.
20 M. Naguib, M. W. Barsoum and Y. Gogotsi, *Adv. Mater.*, 2021, **33**, 2103393.
21 A. Bandyopadhyay, D. Ghosh and S. K. Pati, *Phys. Chem. Chem. Phys.*, 2018, **20**, 4012–4019.
22 P. Zheng, X. Zhang, M. Yan, Y. Ma, Y. Jiang and H. Li, *Appl. Surf. Sci.*, 2021, **550**, 149310.
23 Y. Luo, S. Jia, Y. Yi, X. Liu, G. Zhang, H. Yang, W. Li, J. Wang and X. Li, *J. Alloys Compd.*, 2024, **977**, 173355.
24 T. Chen, T. Zhang and H. Li, *TrAC, Trends Anal. Chem.*, 2020, **133**, 116113.
25 M. He, X. Jin, X. Zhang, X. Duan, P. Zhang, L. Teng, Q. Liu and W. Liu, *Green Chem.*, 2023, **25**, 6561–6580.
26 B. C. Wyatt, S. K. Nemani, K. Desai, H. Kaur, B. Zhang and B. Anasori, *J. Phys.: Condens. Matter*, 2021, **33**, 224002.
27 E. Azadi, N. Singh, M. Dinari and J. S. Kim, *Chem. Commun.*, 2024, **60**, 2865–2886.
28 W. Yang, B. Huang, L. Li, K. Zhang, Y. Li, J. Huang, X. Tang, T. Hu, K. Yuan and Y. Chen, *Small Methods*, 2020, **4**, 2000434.
29 X. Zhao, A. Vashisth, E. Prehn, W. Sun, S. A. Shah, T. Habib, Y. Chen, Z. Tan, J. L. Lutkenhaus and M. Radovic, *Matter*, 2019, **1**, 513–526.
30 J. Tan, B. Fan, P. Zhang, Y. Wei, R. A. Soomro, X. Zhao, J. Kumar, N. Qiao and B. Xu, *Small Methods*, 2024, **8**, 2301689.
31 V. Natu and M. W. Barsoum, *J. Phys. Chem. C*, 2023, **127**, 20197–20206.
32 J. Tan, B. Fan, P. Zhang, Y. Wei, R. A. Soomro, X. Zhao, J. Kumar, N. Qiao and B. Xu, *Small Methods*, 2024, **8**, 2301689.
33 B. Fan, X. Zhao, P. Zhang, Y. Wei, N. Qiao, B. Yang, R. A. Soomro, R. Zhang and B. Xu, *Adv. Sci.*, 2023, **10**, 2300273.
34 L.-Å. Näslund, E. Kokkonen and M. Magnuson, *Appl. Surf. Sci.*, 2025, **684**, 161926.
35 A. Bhat, S. Anwer, K. S. Bhat, M. I. H. Mohideen, K. Liao and A. Qurashi, *npj 2D Mater. Appl.*, 2021, **5**, 61.
36 J. Kumar, R. A. Soomro, B. Fan, J. Tan, N. Sun and B. Xu, *J. Alloys Compd.*, 2024, **1009**, 176749.
37 B. Zhang, P. W. Wong, J. Guo, Y. Zhou, Y. Wang, J. Sun, M. Jiang, Z. Wang and A. K. An, *Nat. Commun.*, 2022, **13**, 3315.
38 X. Wang, Z. Wang and J. Qiu, *Angew. Chem., Int. Ed.*, 2021, **60**, 26587–26591.
39 A. Iqbal, J. Hong, T. Y. Ko and C. M. Koo, *Nano Convergence*, 2021, **8**, 9.
40 A. Jolivet, C. Labbé, C. Frilay, O. Debieu, P. Marie, B. Horcholle, F. Lemarié, X. Portier, C. Grygiel, S. Duprey, W. Jadwisienczak, D. Ingram, M. Upadhyay, A. David, A. Fouchet, U. Lüders and J. Cardin, *Appl. Surf. Sci.*, 2023, **608**, 155214.
41 H.-J. Zhai and L.-S. Wang, *J. Am. Chem. Soc.*, 2007, **129**, 3022–3026.
42 S. Sunderiya, S. Suragtkhuu, S. Purevdorj, T. Ochirkhuyag, M. Bat-Erdene, P. Myagmarsereejid, A. D. Slattery, A. S. R. Bati, J. G. Shapter, D. Odkhuu, S. Davaasambuu and M. Batmunkh, *J. Energy Chem.*, 2024, **88**, 437–445.
43 B. Chang, Y. Guo, D. Wu, L. Li, B. Yang and J. Wang, *Chem. Sci.*, 2021, **12**, 11213–11224.
44 R. Cheng, J. Wang, T. Hu, Y. Zhao, Y. Liang, X. Wang and Y. Zhou, *J. Mater. Sci. Technol.*, 2023, **165**, 219–224.